Modelling of turbulent fluctuations measured in the TCV tokamak with gyrokinetic simulations and a synthetic phase contrast imaging diagnostic

A. Iantchenko[1], G. Merlo[2], S. Coda[1], S. Brunner[1]

[1] *EPFL-SPC, Lausanne, Switzerland*

[2] *University of Texas at Austin, Austin, United States*

We report on progress in modelling localised measurements of turbulent electron density fluctuations obtained with the tangential phase contrast imaging (TPCI) diagnostic installed in the TCV tokamak. Nonlinear flux-tube gyrokinetic (GK) simulations are performed with the Eulerian (grid-based) GENE code [1], taking into account realistic TCV geometry and profiles. A synthetic TPCI diagnostic, developed in MATLAB, is applied as a postprocessing tool to the simulated density fluctuations to model the experimental measurement procedure, allowing detailed comparison between simulation and experiment. In this contribution we test the sensitivity of the results generated by this modelling procedure, in a positive triangularity TCV discharge, to experimental measurement errors in the input density gradient, which provides the main drive of the dominant instability in the considered scenario, the Trapped Electron Mode (TEM). We also make first estimates of electron scale turbulence measurements that are envisioned to be performed, as a result of an upgrade to the TPCI system currently underway.

In the #54990 scenario under study the TPCI measurement is averaged over the range $\rho \sim 0.7$ to 0.9, where ρ is the square root of the normalised toroidal flux. While global simulations would be preferable, we simplify and perform local GK simulations around the flux surface labelled with $\rho = 0.72$. The simulation box is described by the field-line-following coordinate system x, y, z where x is the radial and y the binormal coordinate, while z is the straight-field-line poloidal angle parametrising the position along a given field line. The experimental magnetic geometry provided with the MHD code CHEASE [2] is used in the simulation. At the last closed flux surface, this TCV discharge is characterised by triangularity $\delta = 0.56$, elongation $\kappa \approx 1.35$, magnetic field $B \approx 1.4$T, plasma current $I_p = 258$kA and 0.9MW of central ECH heating. At $\rho = 0.72$ it has safety factor $q_0 = 1.67$, minor radius $a = 0.28$m, major radius $R = 0.89$m and magnetic shear $\hat{s} = 1.61$. To study the effect of the gradients we consider a computationally less expensive case and neglect impurities, electromagnetic effects and collisions in the nonlinear GK simulations. Collisions and impurities were linearly found to have a large stabilising effect and will later have to be included to perform an accurate comparison with experimental results, which is not yet the aim of this contribution. Electromagnetic effects were found to have a very small impact on the linear growth rates. We consider electrons and deuterium ions with

ion-electron temperature ratio $T_i/T_e = 0.43$, and reference electron temperature and density $T_e = 0.4\text{keV}$, $n_e = 1.56\times10^{19}/\text{m}^3$ respectively. The normalised temperature gradient length scale is $R/L_{T_i} = 6.40, R/L_{T_e} = 14.04$ and three values are considered for the density gradient, all within experimental error bars, $R/L_n = \{3.25, 5.43, 7.9\}$, which correspond to three different simulations that we label as the 'low', 'medium' and 'large' density gradient cases respectively. For these nonlinear ion scale simulations we consider a simulation box $L_x \times L_y \sim 128\rho_i \times 126\rho_i$ where ρ_i is the ion sound Larmor radius. The number of (k_x, k_y) modes is $N_x \times N_y = 128\times32$ such that $\max(k_y) = 0.8/\rho_i$ where k_y is an estimate of the poloidal wave number. We consider also $N_z \times N_{v_\parallel} \times N_\mu = 32\times72\times8$, with $v_\parallel$ and the magnetic moment $\mu = mv_\perp/(2B)$ (m is the mass of the species and $B = |\mathbf{B}|$) used to discretise the velocity space parallel and perpendicular to the local magnetic field $\mathbf{B}$ respectively. The extension of the simulation box in velocity space is set to the standard values $L_{v_\parallel} \times L_\mu = 3v_{T_i} \times 9T_e/B$, provided in units of the local ion thermal velocity $v_{T_i} = \sqrt{2T_i^2/m_i}$. A very small $\beta_e = 0.01\%$ (significantly smaller than the experimental value $\beta \approx 0.13\%$) is assumed in order to avoid resolving the high-frequency electrostatic wave generated from the shear Alfvén wave in the limit $\beta_e \to 0$ [3] that significantly slows down the computational time. Adaptive hyperdiffusivities [4] in x and y are used to simulate damping provided otherwise by small-scale modes that are not included in this simulation. All nonlinear simulations are performed for a sufficiently long time, $t_{\text{sim}} > 300\text{R}/\text{c}_\text{s}$ where $c_s = \sqrt{T_e/m_i}$ is the sound speed, for later analysis with the synthetic diagnostic.

The nonlinarly simulated flux surface averaged electron heat flux, multiplied by the area of the enclosing flux surface, is $Q_{\text{large}} \approx 30\text{MW}, Q_{\text{medium}} \approx 23\text{MW}$ and $Q_{\text{low}} \approx 17\text{MW}$, almost doubling from the low to the large gradient case and highlighting the difficulty in using only this quantity for simulation-experiment comparison. Transport in all cases is primarily in the electron channel ($Q_e/Q_i \sim 4.5$ in all cases), consistent with TEM turbulence being dominant for the considered wave numbers as verified by preparatory linear simulations. The increase in the heat flux with increasing density gradient is correlated with an increased growth of the TEM instability as confirmed by these linear simulations.

We apply now the synthetic diagnostic to simulate the experimental TPCI observations of the electron density fluctuations δn_e integrated over a length L, $\int_L \delta n_e \text{d}z$ determined by a spatial localisation technique [5]. We assume a linear detector array consisting of 30 square elements is used to measure fluctuations captured by the 5cm wide beam, such that the maximum measurable wave number is $\max(k_{x_\perp}) = 18.8\text{cm}^{-1}$. Here $x_\perp$ denotes a coordinate locally perpendicular to the TPCI beam and the magnetic field, which is primarly in the radial direction. The smallest measurable wave-number is $k_c = \pm1.01\text{cm}^{-1}$ according to the instrumental transfer function.

The conditional wave number and frequency spectrum $S(k_{x_\perp}|F)$ [5] is shown in Fig. 1. For

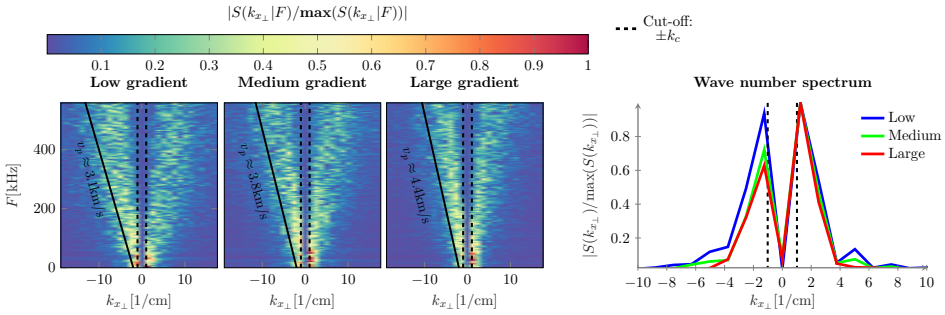

Figure 1: From left to right: conditional wave number and frequency spectrum $S(k_{x_\perp}|F)$ for the low, medium and large gradient case. Solid lines indicates an estimate of the phase velocity of the fluctuations. In the rightmost figure an integration over frequency in the full spectrum has been made, providing the wave number spectrum $S(k_{x_\perp})$. Black dashed lines indicate the lower cut-off wave-number k_c of the phase contrast technique.

all three values of the gradient the spectra are characterised by two branches, representing modes propagating in the positive ($k_\perp > 0$) and negative ($k_\perp < 0$) $x_\perp$ directions respectively. Increasing the gradient increases the phase velocity of the fluctuations from ~ 3.1km/s to ~ 4.4km/s as is indicated by the increase in the slope $\left(2\pi F/k_{x_\perp}\right)$. An integration of the full spectrum $S(F, k_{x_\perp}) = S(k_{x_\perp}|F)/S(f)$ over the frequency F provides the wave number spectrum $S(k_{x_\perp})$ highlighting that effect of increasing the gradient: in addition to increasing the fluctuation amplitude, structures propagating in the positive $x_\perp$ direction are enhanced.

Finally we report on initial results obtained from modelling electron temperature gradient (ETG) scale turbulence in the positive triangularity #54990 discharge. The same resolution is used, but now $L_x \times L_y = 120\rho_e \times 251\rho_e$, where ρ_e is the electron sound Larmor radius. We consider only the low gradient case, and as before neglect electromagnetic effects, collisions and impurities, and additionally ions are assumed to respond adiabatically. We find that background flow shear is required to reduce the size of the turbulent structures which are otherwise very elongated radially and exceed the simulation box size length L_x. Setting the box size and including only the background flow shearing rate $\omega_{E\times B} \approx 1.58 c_s/R$ as measured experimentally by the CXRS diagnostic, is not sufficient. Instead we consider also the shearing rate generated by zonal flows, spatially and temporally averaged, as obtained from the corresponding ion scale simulations. It can be argued that this effect would contribute to the shearing of ETG structures in a more realistic multiscale simulation. The combined zonal flow and background shearing $\omega_{E\times B} \approx 3.5 c_s/R$ reduce substantially the radial correlation length of the structures shown on the left of Fig. 2 and lead to a saturated simulated nonlinear heat flux level, $Q_{\mathrm{ETG}} \sim 2.81$MW, which is significantly lower than the heat flux obtained in the ion scale simulations, yet not negligible.

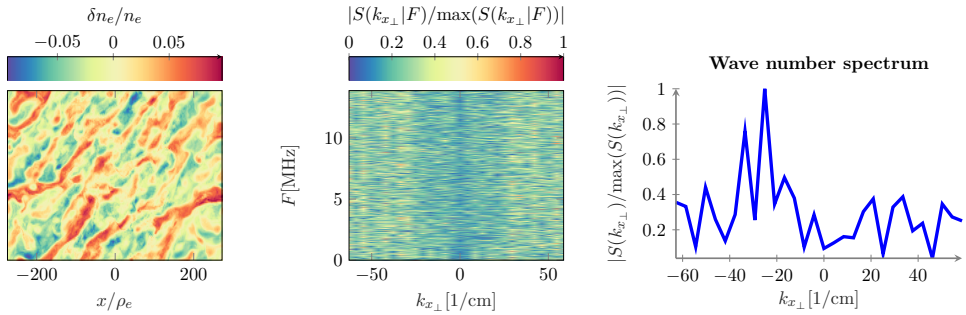

Figure 2: Contours of density fluctuations reduced by background and zonal flow shear (left), conditional wave number and frequency spectrum (medium), and the corresponding wave number spectrum after integrating the full spectrum over the frequency (right).

In the synthetic diagnostic we take the detector planned for the upgraded TPCI set-up for measuring ETG scale turbulence which includes 64 instead of 30 detector elements. In addition, only a 3cm wide portion of the laser beam is exactly projected onto the detector array such that the maximum measurable wave number is $\max(k_{x_\perp}) \sim 67\text{cm}^{-1}$. A first estimate of the frequency and wave number spectrum of the experimental ETG measurement is computed with the synthetic diagnostic, Fig. 2, and reveals a multitude of scattered modes. It is difficult to identify any dominant branch, but a summation over the frequency shows that the component at $k_{x_\perp} \approx -31\text{cm}^{-1}$ is dominant. The asymmetry in the spectrum suggests that structures tend to move preferentially in the negative than in the positive $x_\perp$ direction.

The results presented here are part of the ongoing work to understand the role of plasma triangularity in stabilising turbulence, using detailed simulation-experiment comparison. We plan to investigate the sensitivity in the modelling results also to variations in other input parameters, extend it to the ETG scales and perform all simulations also for a negative triangularity case. Furthermore we will add impurities and collisional effects and attempt to match the experimental results.

The numerical simulations have been carried out on the EUROfusion High Performance Computer (MarconiFusion). This work has been carried out within the framework of the EUROfusion Consortium and has received funding from the Euratom research and training programme 2014-2018 and 2019-2020 under grant agreement No 633053. The views and opinions expressed herein do not necessarily reflect those of the European Commission. This work was supported in part by the Swiss National Science Foundation.

References

[1] F. Jenko, W. Dorland, M. Kotschenreuther, and B. N. Rogers, Physics of Plasmas **7**, 1904 (2000).

[2] H. Lütjens, A. Bondeson, and O. Sauter, Computer Physics Communications **97**, 219 (1996).

[3] W. W. Lee, J. L. V. Lewandowski, T. S. Hahm, and Z. Lin, Physics of Plasmas **8**, 4435 (2001).

[4] M. Pueschel, T. Dannert, and F. Jenko, Computer Physics Communications **181**, 1428 (2010).

[5] C. A. de Meijere *et al.*, Plasma Physics and Controlled Fusion **56**, 072001 (2014).